Improving Rotorcraft Aerodynamics Using Computational Fluid Dynamics

J. Beedy, G. Barakos, K. Badcock, & B. Richards

CFD Laboratory
University of Glasgow
Department of Aerospace Engineering
Glasgow G12 8QQ
United Kingdom
www.aero.gla.ac.uk/Research/CFD

Abstract

In current practice, the design of helicopter rotors is based on reduced aerodynamic models calibrated against experimental data while the use of computational fluid dynamics (CFD) by the industry is still restricted. In recent years, however, progress in CFD methods combined with the rapid increase of computing power has made a significant impact on the analysis and understanding of unsteady flow phenomenon. It is now possible to perform a complete analysis of a rotor using the Navier-Stokes equations and appropriate turbulence modelling. It is equally possible to couple the fluid-flow analysis with a structural model of the rotor in order to model the complete dynamics of the system. Despite this progress, two issues remain concerning the adoption of CFD by the industry as a design tool. Firstly, the CPU time required to run full unsteady calculations is still prohibitive to industry, and secondly, there is still much validation needed of the numerical and turbulence modelling schemes employed in CFD.

With the use of relatively new field methods like Laser Doppler Velocimetry (LDV) and triple hot-film probes to obtain detailed information about the velocity field within the tip vortex of unsteady laminar and turbulent flows, it is now possible to validate CFD solutions for more complex regions of the flow field. The work of Chang *et al.* [5] is used in the present research program to provide direct validation of the PMB code. The experiments by Ramaprian *et al.* [7] provide a case with a Reynolds number high enough to require a turbulence model. The problem studied in both cases is the behaviour of the tip vortex as it evolves from the tip of an oscillating square wing. Of significant importance is the trajectory of the vortex as well as the relationship between the motion of the vortex and the motion of the wing. Further CFD results for the oscillating cases for the rectangular wing, corresponding to the further work of Ramaprian *et al.* [8], indicate that the position of the vortex follows the motion of

the wing at a fixed phase angle.

Nomenclature

c	Chord length of the airfoil
C_p	Pressure coefficient, $C_p = \frac{1}{2\rho U_\infty^2}(P - P_0)$
x	Chordwise coordinate axis
y	Normal coordinate axis
z	Spanwise coordinate axis
k	Reduced frequency of oscillation, $k = \frac{\omega c}{U_\infty}$
M	Mach number
Re	Reynolds number, $Re = \rho U_\infty c/\mu$
U	Local Axial Velocity
U_∞	Free-stream axial velocity

Greek Symbols

α	Incidence
α_0	Mean incidence for oscillatory cases
α_1	Amplitude of oscillation
μ	Viscosity
ρ	Density
ρ_∞	Density at free-stream
ω	Oscillation Frequency

Introduction

The near and wake vortex flow structures generated by both fixed wing and rotary wing aircraft is a complex and challenging area of aerodynamics. The importance of the flow in this region is highlighted even in elementary textbooks of aerodynamics since it is associated with the downwash and induced drag of wings. Since the flow structure near the tip plays a key role in the performance of both fixed and rotary wing vehicles, experimental [2, 3, 4, 5, 6, 7, 8, 9] theoretical [10, 11, 12, 13, 14] studies of this region have been conducted. Starting from the theoretical work conducted so far, one cannot fail to notice that most of the published Computational Fluid Dynamics (CFD) studies have considered only steady flow conditions and our knowledge of the simulation of unsteady tip flows which have not been attempted. Experimental work on the other hand, has tried to generate understanding of the basic phenomenon of the formation of the tip vortex. It is, however, evident that most of the generated results are not suitable for validation of CFD since only qualitative data are presented from flow visualisation.

The present CFD study focuses, primarily, on the region near the wing tip where the tip vortex is generated. This type of study is rare using CFD with only a few exceptions [12, 14]. As mentioned earlier, qualitative data are available from a number of experiments [5, 6, 7, 8, 9], however experiments allowing for quantitative comparisons against CFD are very limited. For most cases, even if some data are available these are often restricted to surface pressure measurements and little or no data exist for the flow field within the tip vortex.

The primary objective of this paper is to present the validation work regarding the unsteady tip vortex during roll-up, and thereby to provide a basis for further investigations using CFD. Using the work of Chang *et al.* [4] of Ramaprian *et al.* [2, 3] laminar and turbulent flows and steady and oscillating wing tips have been computed. The employed test cases used Laser Doppler Velocimetry (LDV) and triple hot-film probes in order to obtain quantitative data for the velocity fields within the of the tip vortex region. This data is then used as the initial part of the CFD validation process.

Employed CFD Tools

The CFD solver used for this study is the PMB code developed at the University of Glasgow [1]. The code is capable of solving flow conditions from inviscid to laminar to fully turbulent using the Reynolds Averaged Navier-Stokes (RANS) equations in three dimensions. These equations are non-dimensionalised and transformed from a Cartesian reference system to a curvilinear one before being solved. The use of the RANS form of the equations allows for fully turbulent flow conditions to be calculated with appropriate modelling of turbulence. The turbulence model used for this study is the standard $k-\omega$ model [15]. To solve the RANS equations, a multi-block grid is generated around the required geometry, and the equations are discretised using the cell-centered finite volume approach. Convective fluxes are discretised using's Osher upwind scheme, which is used because of its robustness, accuracy and stability properties. Viscous fluxes are discretised using central differences. Boundary conditions are set using sets of halo cells. The solution is marched implicitly in time using a second-order scheme and the final system of algebraic equations is solved using a conjugate gradient method.

Validation Cases

Although several experimental investigations exist for flows over oscillating aerofoils and wings very few cases were suitable for this study. This is because most of the experiments focus on measuring surface pressure distributions while measurements of the wake and the tip vortices behind the wing are very rate. The first test case is based on the experiments of Lee et al. [4]. These oscillatory experiments were conducted in a closed-circuit wind tunnel, using a 10% square NACA 0012 profile wing section. The flow conditions are entirely laminar which means there is no requirement for a turbulence modelling thus making this case ideal for initial validation of CFD.

The second test case is based on the work of Ramaprian et al. [2,3]. The experiments consider the flow around both steady and oscillating wings, with the aim of studying the evolution of the tip vortex from a square NACA 0012 wing section.

A summary of the test cases is presented in Tables 1 and 2. Amongst many experimental investigations these appear to be the most comprehensive in terms of the measured quantities, and therefore, are the most suitable for CFD validation.

Research Discussion

Laminar Test Cases

For the laminar case (Case 1 of Table 2), experimental data are only available for oscillating wing cases. The flow conditions were set the same as for the experimental case. The experimental and computational results are presented in Figures 1 and 2. Contours are shown for the non-dimensional axial velocity $\left(\frac{U}{U_\infty}\right)$ behind the wing at two different distances $x/c = 0.5$ and $x/c = 1.5$ and for an incidence of $\alpha = 11\ deg.$ during the pitch-up and pitch-down parts of the oscillation cycle. For all the CFD results presented, contours have been drawn between the limits indicated by the experiments, and the same number of contours is used to ensure as accurate a comparison between the results as possible. For all cases the vortex core is predicted to be close to the experimental location. On the same figures

the relative position of the wing is also presented. The obtained results suggest that the tip vortex follows the motion of the wing in phase with the imposed oscillation. The dissipation of the numerical scheme was found to have little influence up to a distance of 5 chords behind the wing where the employed grid was indeed too coarse to preserve the strength of the vortex. Pressure contours are presented on Figure 3 and again results are shown for $x/c = 0.5$ and $x/c = 1.5$ at incidences of 11 deg pitch-up and pitch down during the oscillation cycle. The suction near the centre of the vortex is shown to induce a significant distortion in the pressure field especially on the plots for $x/c = 0.5$. Overall, the numerical predictions were found to agree remarkably well with the measurements apart from the region very close to the vortex core. On the other hand, the accuracy of the LDV measurements in this region is also limited due to the difficulty in accurately locating the core and measuring in a relatively slow flow.

Turbulent Test Cases

For the turbulent cases (Cases 2 and 3 from Table 2), both steady and unsteady results are included. For the steady case, the flow conditions used for computations are set to those of the experiments of Ramaprian *et al.* [2] as outlined earlier. For the unsteady case the incidence varied harmonically as reported in [3].

The steady flow case (Figures 4 and 5) shows the tip vortex at four stations rear-wards from the trailing edge. The stations correspond to distances from the trailing edge tip As was the case for the laminar predictions, the CFD results are in fair agreement with the experiments as far as the strength of the vortex, and its position are concerned. A grid of about 1 million points was used for this case, since we had to resolve in detail the turbulent boundary layers on the wing as well as the near-tip flow region. The CPU time required for this was about 3830 CPU minutes and calculation were performed on a 6-node Beowulf cluster of Athlon processors.

For the unsteady flow case (Case 3 of Table 2), results are presented in Figures 6 and 7. Contours of the non-dimensionalised axial velocity $\left(\frac{U}{U_\infty}\right)$ are presented for four time instances corresponding to incidences of 5 deg and 10 deg during the up-stroke, and 15 deg and 10 deg during the down-stroke. The CFD plots (Figure 7) were selected to match the conditions of the figures published in [3] which are also shown here on Figure 6. For all plots the vortex structure is presented at a distance of $x/c = 0.67$ behind the trailing edge, and the trailing edge position is represented by the dashed line in all cases. All figures include the maximum and minimum non-dimensional axial velocity for each point in the oscillation cycle. The relative position of the vortex with respect to the wing is well predicted and the same is true for the overall shape of the vortex. This is a very encouraging result given the complexity of this unsteady flow. A much better representation of the evolution of the unsteady vortex is shown in Figure 8, where pressure contours are shown for the same four incidences. At 5 deg. (Figure 8(a)) we have a small vortex located well above the wing. As the incidence increases and the vortex grows in size (Figure 8(b)) the distance between the vortex and the wing appears to decrease and a minimum is reached for the first down-stroke step (Figure 8(c)). During

the down-stroke part of the cycle the vortex decreases in size reaching a minimum at the minimum incidence encountered during the cycle.

Flow Fields

To understand the effect of the presence of the tip vortex on the loading of the wing, a number of plots have been included for both cases. Figure 9 presents CFD results for the C_p coefficient near the tip. CFD results are shown for three incidences during the oscillation cycle. As the wing passes the first incidence (Figure 9(a)) a minimal disturbance on C_p is observed. The situation changes slightly at an incidence of 15 deg. (Figure 9(b)) where a second peak of the C_p emerges near the downstream corner of the wing. This second peak is lower than the suction peak which dominates the leading edge region of the wing. A steady gradual decay of the C_p is observed as moving from the root to the tip of the wing. Finally, Figure 9(c) shows the variation at the minimum incidence of the cycle (3 deg.). At such an incidence the C_p distribution near the leading edge suggests that stall is encountered. The effect of the vortex again dominant near the trailing edge of the wing where a prominent suction peak is observed.

As with the laminar case, Figure 10 presents the variation of surface C_p with incidence. Results are first presented in Figure 10(a) for an incidence of 5 deg. Before the vortex is weak during this early stage of the oscillation and it has minimal effect on the C_p distribution. Due to the hysteresis of the flow, however, one may not encounter a small second peak in the C_p near the trailing edge of the wing. Figure 10(b) presents results at 10 deg. of incidence. The second peak near the trailing edge is now dominant and is comparable in size with the suction peak near the leading edge. At this stage the vortex is well formed and appears to dominate the flow in the vicinity of the tip. At 15 deg. of incidence (Figure 10(c)) the leading edge of the tip has a much lower C_p than the trailing edge. This is expected since at this stage the vortex has reached a maximum in terms of size and strength.

Conclusions

Numerical simulations have been undertaken for inviscid flows past various wings. All calculations have been performed at steady and steady conditions and geometry symmetry boundary numbers covering laminar and turbulent flows. The CPU time required to resolve this complex flow was found to be small which highlights the efficiency of the CFD solvers. The CFD results were found to compare favourably against experiments reported in the literature for the location of the vortex and the levels of the axial velocity behind the trailing edge. Established some confidence on CFD results an attempt has been made to relate the strength of the vortex and its position with the shape of the C_p distribution near the tip. It appears that the vortex affects significantly the loads on the wing, especially near the trailing edge and effective varies with the incidence. It is clear that experiments report both the surface pressure distribution and the velocity field behind the wing are necessary for further validation of CFD methods for complex unsteady flows.

Acknowledgements

Financial support from Westland Helicopters

Ltd. is gratefully acknowledged.

Bibliography

1. Badcock, K., Richards, B. & Woodgate, M., "Elements of computational fluid dynamics on block structured grids using implicit solvers", *Progress in Aerospace Sciences*, **36**(5-6), pp. 351–92, 2000.

2. Ramaprian, B. & Zheng, Y., "Measurements in Rollup Region of the Tip Vortex from a Rectangular Wing", *AIAA Journal*, **35**(12), pp. 1837–1843, 1997.

3. Ramaprian, B. & Zheng, Y., "Near Field of the Tip Vortex Behind an Oscillating Rectangular Wing", *AIAA Journal*, **36**(7), pp. 1263–1269, 1998.

4. Chang, J.S. & Park, [illegible], "Measurements in the Tip Vortex Roll-Up Region of an Oscillating Wing", *AIAA Journal*, Technical Note, **38**(6), pp. 1092–95, 2000.

5. Singh, P. & Uberoi, M., "Experiments on Vortex Stability", *Physics of Fluids*, **19**(12), pp. 1858-1863, 1976.

6. Green, S. & Acosta, A., "Unsteady Flow in Trailing Vortices", *Journal of Fluid Mechanics*, **227**, pp. 107-134, 1991.

7. Shekarriz, A., Fu, T., Katz, J. & Huang, T., "Near-Field Behavior of a Tip Vortex", *AIAA Journal*, **31**(1), pp. 112-118, 1993.

8. Devenport, W., Rife, M., Liapis, S. & Follin, G., "The Structure and Development of a Wing-tip Vortex", *Journal of Fluid Mechanics*, **312**, pp. 67-106, 1996.

9. Chow, J., Zilliac, G. & Bradshaw, P., "Mean and Turbulence Measurements in the Near Field of a Wingtip Vortex", *AIAA Journal*, **35**(10), pp. 1561–1567, 1997.

10. Spreiter, J. & Sacks, A., "The Rolling Up of the Trailing Vortex and its Effect on the Downwash Behind Wings", *Journal of the Aeronautical Sciences*, pp. 21–32, January, 1951.

11. Phillips, W., "The Turbulent Trailing Vortex During Roll-Up", *Journal of Fluid Mechanics*, **105**, pp. 451–467, 1981.

12. Srinivasan, G. R., McCroskey, W., Baeder, J. & Edwards, T., "Numerical Simulation of Tip Vortices of Wings in Subsonic and Transonic Flows", *AIAA Journal*, **26**(10), pp. 1153–1162, 1998.

13. Zeman, O., "The Persistence of Tailing Vortices A modeling Study", *Physics of Fluids*, **7**(1), pp. 135–143, 1995.

14. Dacles–Mariani, J., Zilliac, G., Chow, J. & Bradshaw, P., "Numerical/Experimental Study of a Wingtip Vortex in the Near Field", *AIAA Journal*, **33**(9), pp. 1561–1568, 1995.

15. Wilcox, D.C., "Reassessment of the Scale-Determining Equation for Advanced Turbulence Models", *AIAA Journal*, **26**(11), pp. 1299-1310, 1988.

No	Test Case	Wing Geometry
(1)	Chang *et al.* [4]	rectangular planform, NACA 0012 profiles, zero twist
(2)	Ramaprian *et al.* (Steady) [2]	rectangular planform, NACA 0015 profiles, zero twist
(3)	Ramaprian *et al.* (Oscillating) [3]	rectangular planform, NACA 0015 profiles, zero twist

Table 1: Description of the wing geometry for the employed test cases.

No	Re	Mach Number	Turbulence Model	α_0 $(deg.)$	α_1 $(deg.)$	Reduced Frequency	Axis of Rotation	Grid Size
(1)	3.4×10^4	0.15	Laminar	15	15	0.09	$x/c = 0.25$	$800,000$
(2)	1.8×10^5	0.15	$k-\omega$	-	-	-	$x/c = 0.25$	$1,000,000$
(3)	1.8×10^5	0.15	$k-\omega$	10	5	0.10	$x/c = 0.25$	$1,000,000$

Table 2: Summary of conditions for the employed test cases.

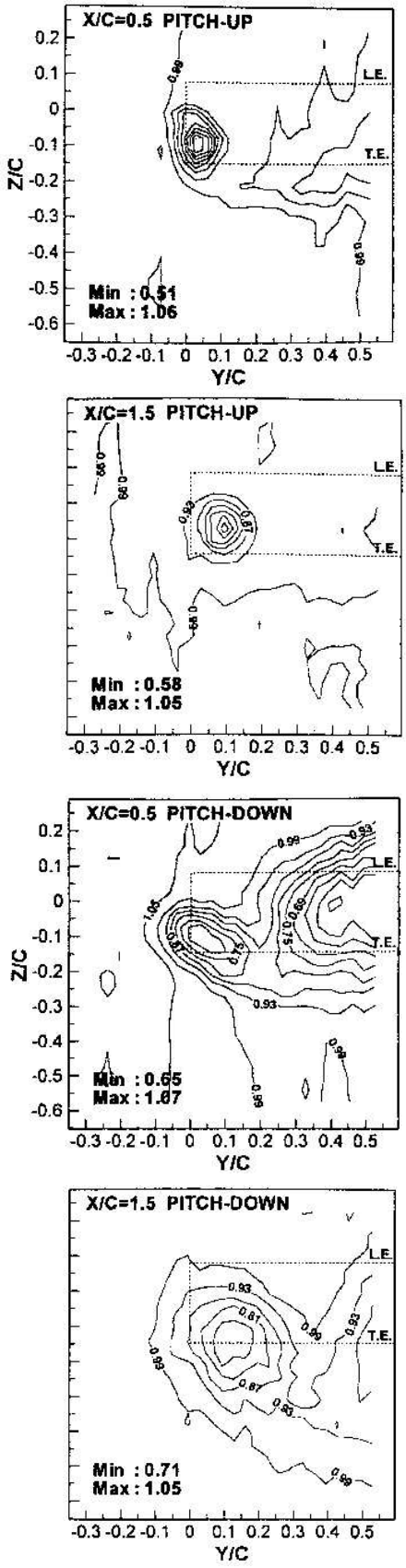

Figure 1: Experimental results from [4] for the non-dimensional axial velocity in tip vortex. The conditions of the test correspond to the Test Case 1 reported in Table [2].

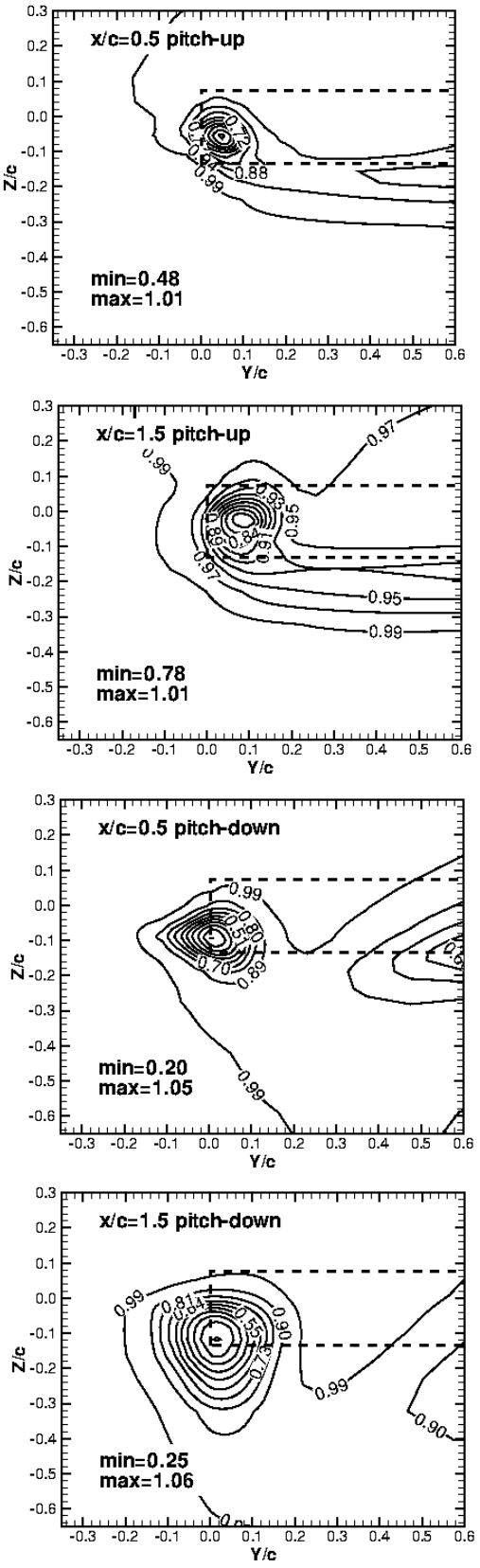

Figure 2: CFD results for the non-dimensional axial velocity in tip vortex. The conditions of the test correspond to the Test Case 1 reported in Table [2].

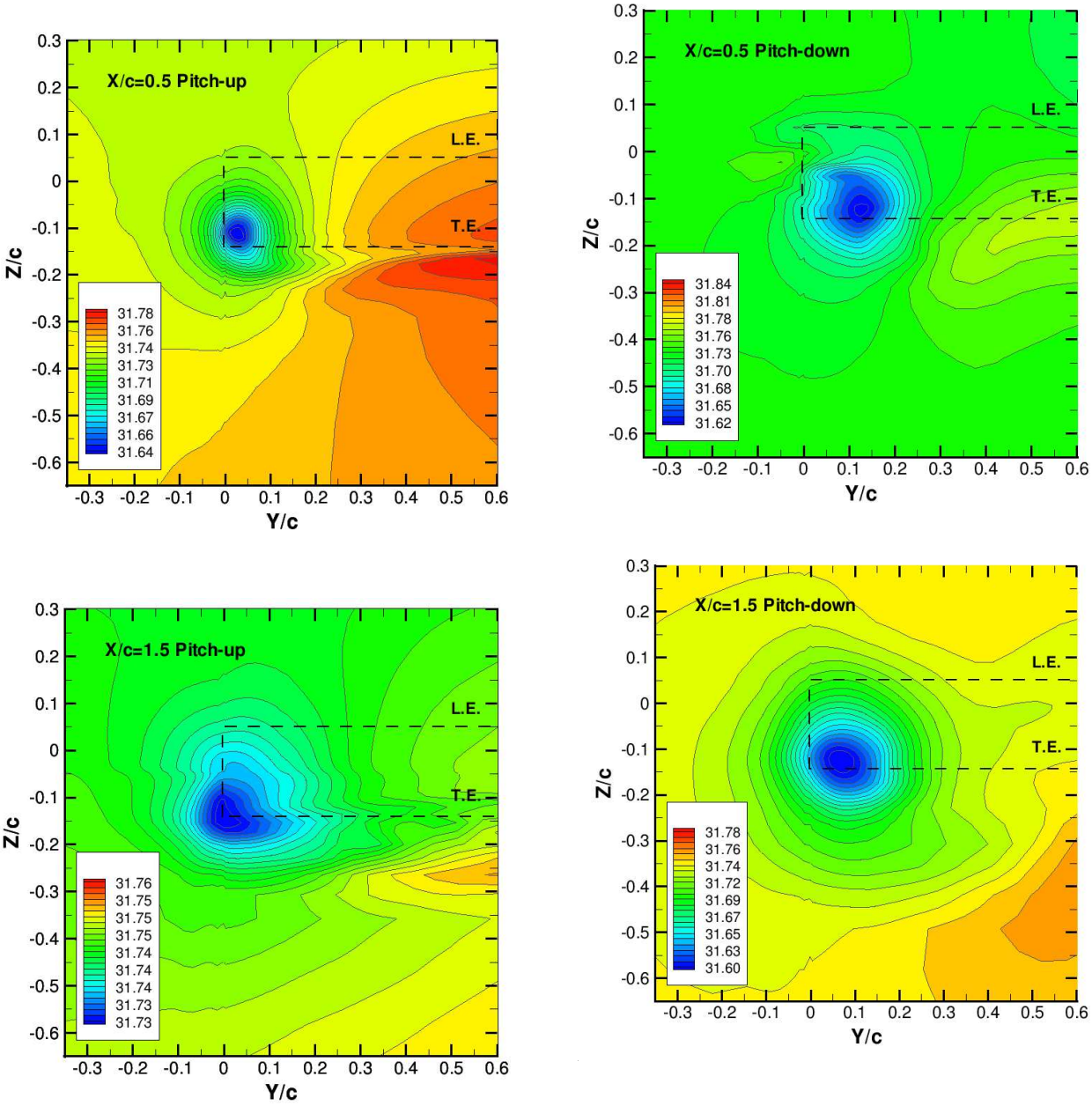

Figure 3: Contours of non-dimensional pressure $\frac{P}{\rho U_\infty^2}$ calculated using CFD within tip vortex. The conditions of the calculations correspond to the experiment of Chang *et al.* [4] (see Test Case 1 in Table [2]).

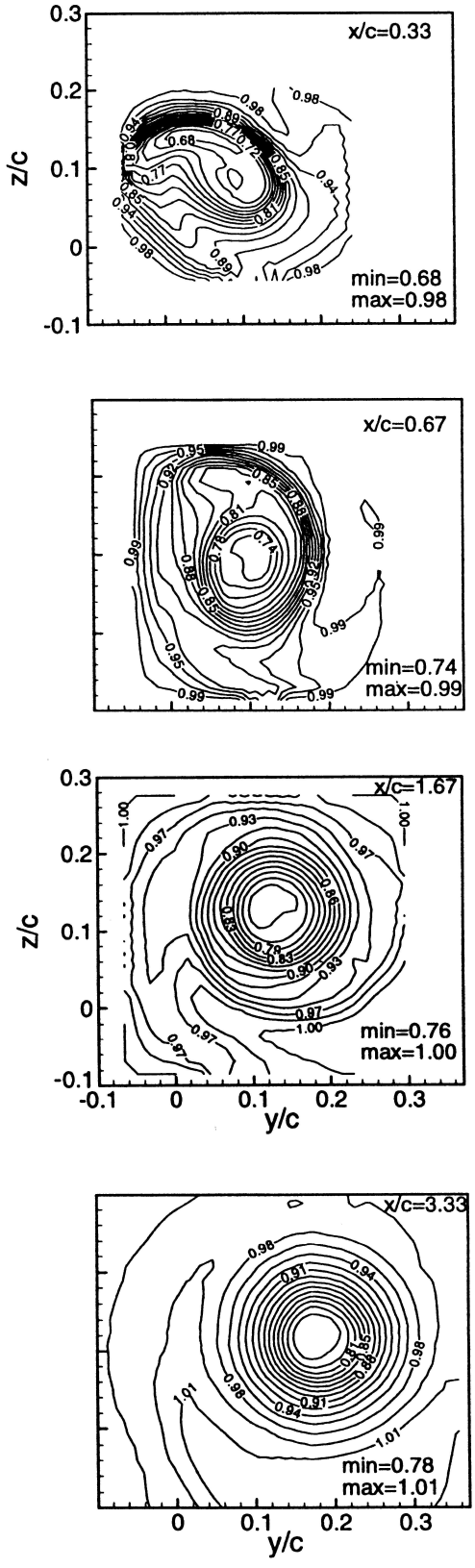

Figure 4: Experimental results from [2] for the non-dimensional axial velocity in tip vortex. The conditions of the experiment correspond to the Test Case 2 reported in Table [2].

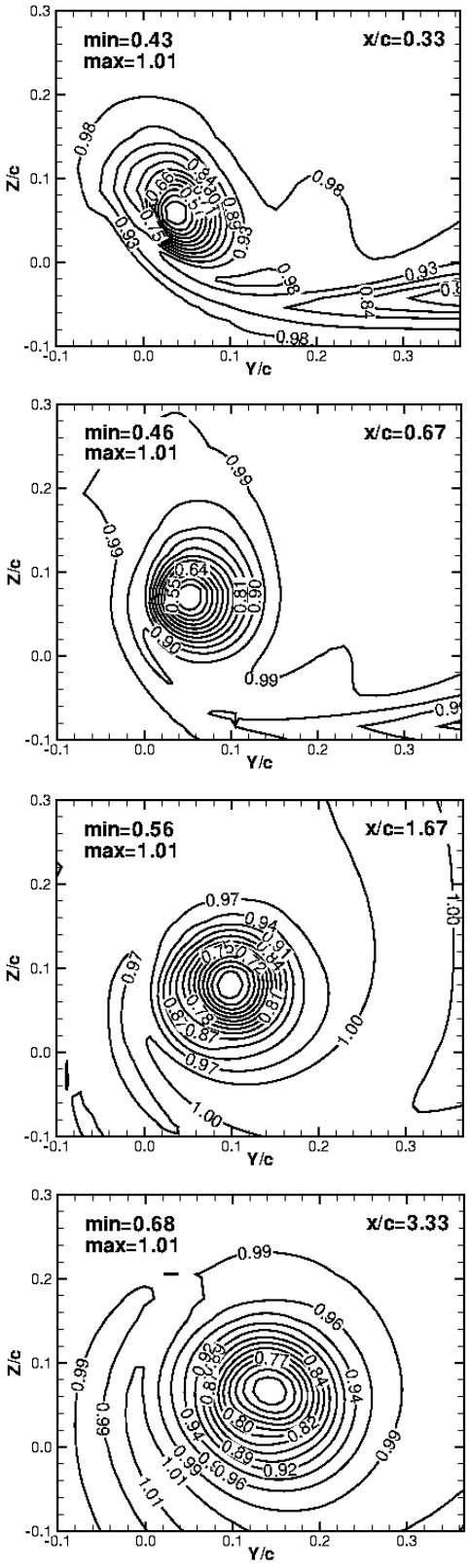

Figure 5: CFD results for the non-dimensional axial velocity in tip vortex. The conditions of the computations correspond to the Test Case 2 reported in Table [2].

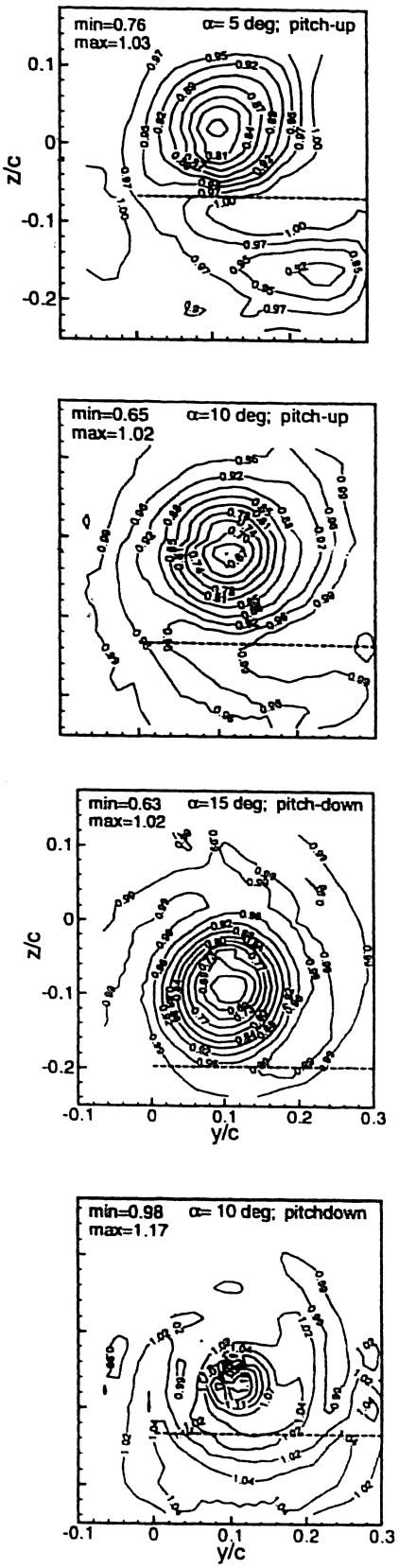

Figure 6: Experimental results from [3] for the non-dimensional axial velocity in tip vortex. The conditions of the test correspond to the Test Case 3 reported in Table [2].

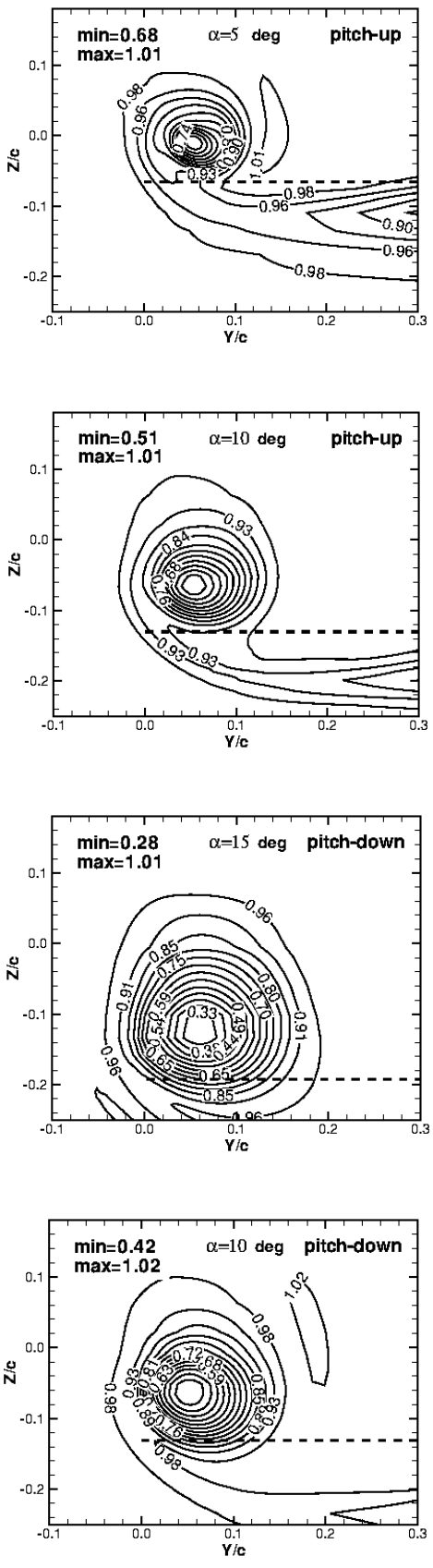

Figure 7: CFD results for the non-dimensional axial velocity in tip vortex. The conditions of the test correspond to the Test Case 3 reported in Table [2].

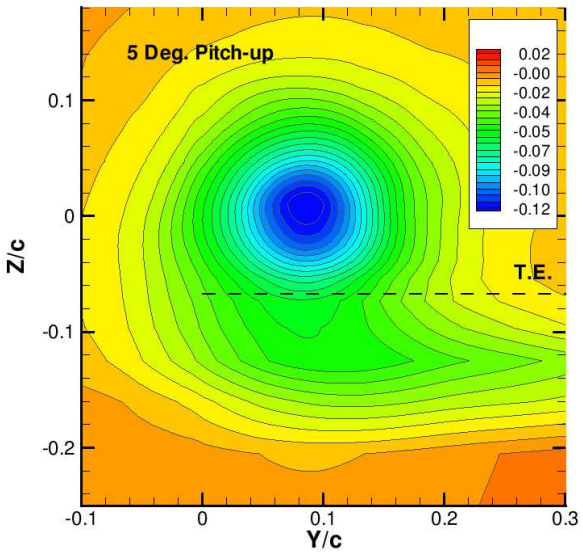

(a)

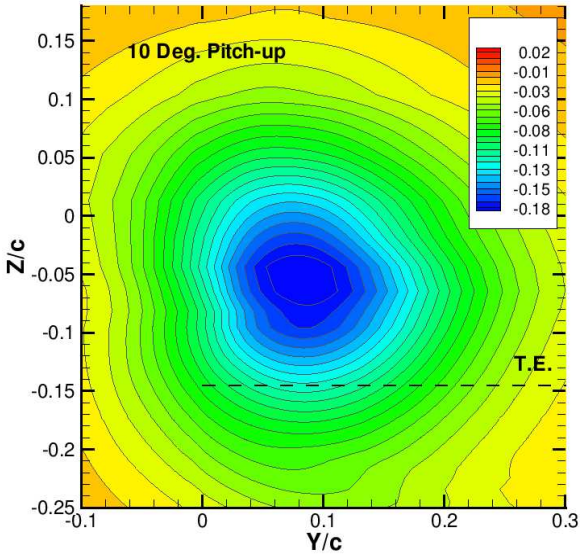

(b)

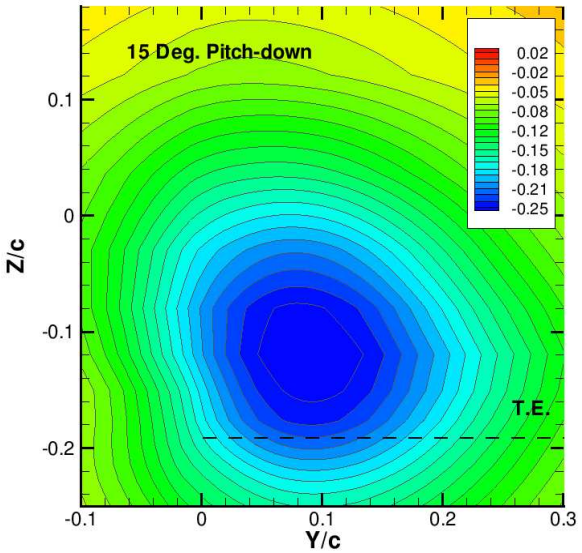

(c)

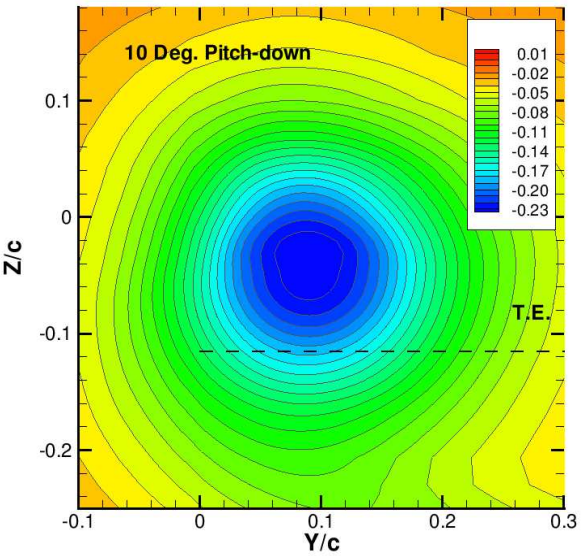

(d)

Figure 8: Contours of pressure coefficient (C_p) calculated using CFD within tip vortex. The conditions of the calculations correspond to the experiment of Ramaprian *et al.* [3] (see Test Case 3 in Table [2]).

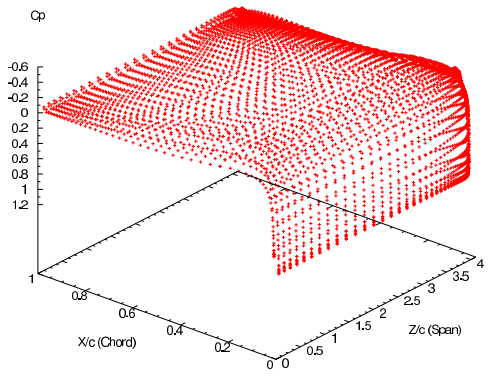

(a)

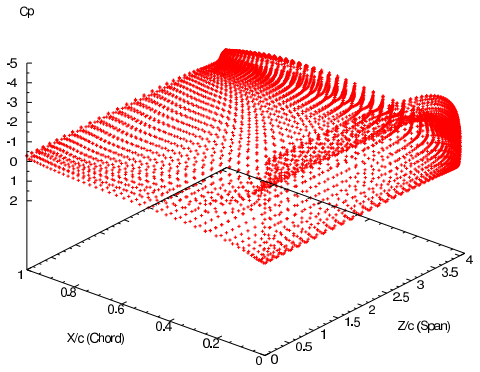

(b)

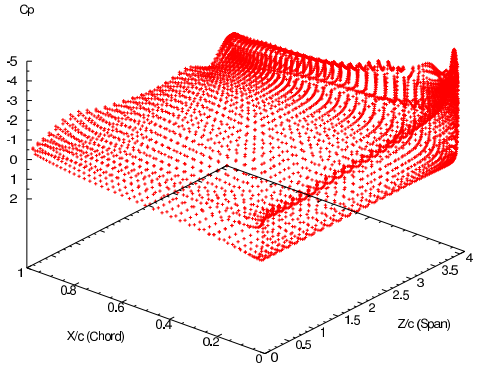

(c)

Figure 9: CFD results for the surface C_P variation for (a) $\alpha = 0\ deg$, (b) $\alpha = 15\ deg$, $\alpha = 30\ deg$ during pitch-up. The conditions correspond to the experiments of Chang *et al.* [4] (see Test Case 1 in Table [2]).

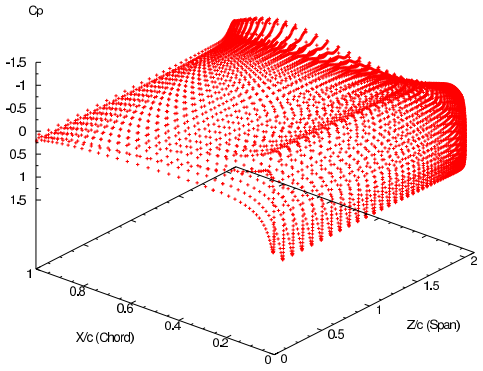

(a)

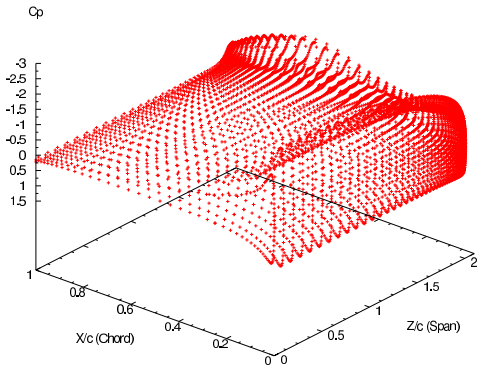

(b)

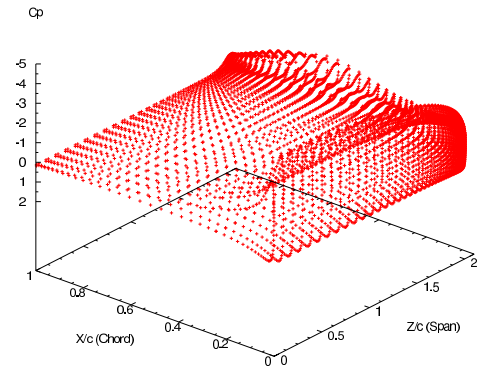

(c)

Figure 10: CFD results for the surface C_P variation for (a) $\alpha = 0\ deg$, (b) $\alpha = 5\ deg$, (c) $\alpha = 10\ deg$, $\alpha = 15\ deg$ during pitch-up. The conditions correspond to the experiments of Ramaprian *et al.* [3] (see Test Case 3 in Table [2]).